The onset of sub-surface oxidation induced by defects in a chemisorbed oxygen layer

Jonathan Li, Liang Li, and Guangwen Zhou

Citation: The Journal of Chemical Physics **142**, 084701 (2015); doi: 10.1063/1.4913237
View online: http://dx.doi.org/10.1063/1.4913237
View Table of Contents: http://scitation.aip.org/content/aip/journal/jcp/142/8?ver=pdfcov
Published by the AIP Publishing

The onset of sub-surface oxidation induced by defects in a chemisorbed oxygen layer

Jonathan Li,[1] Liang Li,[2] and Guangwen Zhou[2,a)]
[1]*Department of Physics, Applied Physics and Astronomy and Multidisciplinary Program in Materials Science and Engineering, State University of New York, Binghamton, New York 13902, USA*
[2]*Department of Mechanical Engineering and Multidisciplinary Program in Materials Science and Engineering, State University of New York, Binghamton, New York 13902, USA*

(Received 30 October 2014; accepted 6 February 2015; published online 24 February 2015)

We investigate the onset of internal oxidation of a Cu(110) surface induced by oxygen subsurface adsorption via defects in the Cu(110)–(2 × 1)–O chemisorbed layer. The presence of a boundary formed by merged add-row structure domains due to a mismatch of half unit-cell leads to preferred oxygen adsorption at the subsurface tetrahedral sites. The resulting distorted Cu–O tetrahedra along the domain boundary have comparable bond length and angles to those of the bulk oxide phase of Cu_2O. Our results indicate that the presence of defects in the oxygen-chemisorbed adlayer can lead to the internal oxidation via the formation of Cu_2O-like tetrahedra in between the topmost and second outermost atomic layers at the oxygen coverage $\theta = 0.53$ and the second and third outermost atomic layers at $\theta = 0.56$. These results show that the internal oxidation of a metal surface can occur in the very beginning of the oxygen chemisorption process enabled by the presence of defects in the oxygen chemisorbed layer. © *2015 AIP Publishing LLC.* [http://dx.doi.org/10.1063/1.4913237]

I. INTRODUCTION

The oxidation of metals has been studied intensively due to its important role for industrial processes, such as chemical catalysis,[1–3] corrosion,[4,5] and high temperature oxidation.[6,7] Surface oxidation also plays a crucial role in copper catalysis such as synthesis of methanol,[8] electroless plating,[9] and fuel cell electrodes.[10] The typical reaction sequence of the surface oxidation of single crystals of copper proceeds according to the following steps. Upon exposure to an oxygen atmosphere, oxygen chemisorption occurs while the surface restructures, followed by oxide nucleation and growth and eventually bulk oxide formation. Incorporation of oxygen atoms through the oxygen chemisorbed layer into the subsurface region is required for initiating the nucleation of a bulk oxide phase for a planar surface. Although much work has been done to understand the structure and kinetics of oxygen chemisorption, unraveling the atomic process underlying the transition from the chemisorption of oxygen at metal surfaces to the formation of a bulk oxide phase remains an ongoing theme. There are still unanswered questions about the effect of oxygen chemisorption on bulk oxide formation. More specifically, the atomic details of oxygen-adsorption induced transformation of the metal crystal lattice in the subsurface region into its oxide are not clearly resolved.

A well-known theoretical notation proposed by King and co-workers[11–15] suggests that a critical oxygen coverage is required at which the transition between a two-dimensional (2D) chemisorbed layer and the appearance of an oxide phase occurs spontaneously. At low oxygen coverage, the heat of formation of the chemisorbed phase is higher than the heat of formation of the oxide. With increasing oxygen coverage, the strong repulsive force between the oxygen atoms in the chemisorbed layer results in a sharp decrease of the heat of adsorption and enables oxygen subsurface site occupation, thereby making oxide formation energetically more favorable than adsorption of extra oxygen at on-surface sites. While this model explains successfully why a critical surface coverage of oxygen is needed for oxide formation,[11–17] it does not account for the microscopic processes underlying the phase transition from the 2D chemisorbed layer to the 3D oxide as well as the effect of defects in the oxygen chemisorbed layer on the oxide formation. In general, there is a lack of study on how defects formed in an oxygen chemisorbed layer influence subsequent reconstructions (if any) by on-surface oxygen uptake and/or oxide formation by subsurface adsorption.

In FCC (face-centered cubic) Cu lattice, two types of interstitial sites, i.e., octahedral and tetrahedral sites, are available for possible subsurface oxygen occupancy. According to density-functional theory (DFT) calculations, the octahedral site is energetically more favorable for oxygen adsorption than the tetrahedral site.[18–22] In Cu_2O structure, oxygen atoms reside at the tetrahedral sites (1/4, 1/4, 1/4) and (3/4, 3/4, 3/4) of FCC Cu lattice. Therefore, the oxygen octahedral site occupancy is not an indication of Cu_2O nucleation. The transformation of oxygen preference from octahedral sites to the tetrahedral sites represents a crucial step in the onset of the bulk oxide (Cu_2O) formation.

The dynamic aspects of the surface restructuring induced by oxygen chemisorption typically show a two-dimensional nucleation and growth mechanism of reconstructed domains, which leads to the formation of reconstructed nanodomains along with a high density of domain boundaries in the

a)Author to whom correspondence should be addressed. Electronic mail: gzhou@binghamton.edu

oxygen chemisorbed layer.[23–28] Scanning tunneling microscopy (STM) observations have shown that oxygen chemisorption results in the formation of domain boundaries in the oxygen chemisorbed layers of the c(2 × 2)–O and (2√2 × 2√2) R45°–O reconstructions[23,28] and oxide islands can form preferentially at the domain boundary areas.[28] While similar atomic-scale STM observations of oxide formation on the reconstructed Cu(110) surfaces are still lacking, it has been shown that oxygen chemisorption on Cu(110) results in the formation of Cu–O–Cu chain fragments that can diffuse and shift laterally by one atomic row in the [110] direction.[29,30] The merging of shifted and un-shifted Cu–O–Cu chains can naturally form domain boundaries. Therefore, we hypothesize that domain boundary defects can form in the Cu(110)–(2 × 1)–O chemisorbed layer by the random nucleation and merging of fragmented and shifted of Cu–O–Cu–O chains and examine the effect of the presence of these domain boundaries on further oxygen adsorption.

Li *et al.* recently proposed a mechanism for oxide nucleation close to a domain boundary defect formed by mismatched missing rows of oxygen-chemisorbed (2√2 × 2√2) R45°–O domains on Cu(100) terraces.[31] Using DFT, they showed that subsurface oxygen adsorption at the tetrahedral site is more favorable than at the octahedral site near the domain boundary at the oxygen coverage θ = 0.53. For a non-defective missing-row reconstructed Cu(100) surface, Lee *et al.* noted that the oxygen tetrahedral adsorption can occur at the oxygen coverage θ = 1 with the presence of an oxygen molecule adsorbed on the reconstructed Cu(100) surface; if the oxygen molecule is absent, no tetrahedral adsorption occurs even at a higher oxygen coverage.[20] Therefore, the presence of the domain boundary defect in the missing-row reconstructed Cu(100) surface promotes Cu_2O nucleation in Cu(100) at a lower oxygen coverage than a non-defective missing-row reconstructed Cu(100) surface. In addition to domain boundary defects promoting subsurface oxygen adsorption, the interface between different phases can also promote subsurface oxygen adsorption. Using STM and XPS, Lahtonen *et al.* determined that the interface between Cu–O islands and the missing row reconstruction on Cu(100) is active towards oxygen penetration into subsurface region.[28]

For some metals, surface oxide phases may exist between the chemisorbed layer and the bulk oxide.[32–35] On Cu, some surface oxide phases include "29",[36,37] "44",[38] and "5-7"[39] on (111), (2√2 × 2√2) R45° missing-row structure on (100),[26,39] and the added (2 × 1)–O structure and c(6 × 2) on (110).[42–44] On Ru(0001), oxidation beyond an initial (1 × 1)–O adlayer phase produces a heterogeneous surface, comprising a disordered trilayerlike surface oxide and an ordered RuO_2 (110) thin-film oxide.[45] Evidence has been provided to show that there is a distinct oxide phase that is the precursor to bulk PdO and PtO_2 formation by bulk oxide formation on top of the metal, which forms as small particles, referred to as seeds, within domains of the coexisting surface oxide.[46–48] Three-dimensional compact Cu_2O islands may also form on the surface of Cu(100) and (110),[49–53] and interfaces between the islands may promote bulk oxide formation in the subsurface.[28] In our work, the precursor to bulk Cu_2O oxide is in the surface oxide phase consisting of a domain boundary formed by merged misaligned Cu–O–Cu–O chains of the Cu(110)–(2 × 1)–O phase.

Oxygen chemisorption on Cu(110) has been studied extensively regarding oxygen adsorption and the resulting surface reconstruction.[18,40–43,54–57] Different from Cu(100), oxygen chemisorption on Cu(110) results in two well-defined reconstructions, an added-row (2 × 1)–O structure with the saturation oxygen coverage θ = 0.5 that transits to a $c(6 \times 2)$ structure with a saturated oxygen coverage θ = 2/3.[42–44] Using DFT calculations, Li *et al.* studied the stability and structural change of the Cu(110)–$c(6 \times 2)$ surface with increasing oxygen coverage and showed that a transition from oxygen octahedral occupancy to tetrahedral preference occurs when the oxygen coverage reaches θ = 1.[58] In this work, we present a systematic investigation of oxygen subsurface adsorption along the domain boundaries formed by the merging of misaligned domains of the Cu(110)–(2 × 1)–O reconstruction. By employing DFT calculations, we explore the domain boundary defect and its effect on Cu_2O nucleation on Cu(110) surface. We show that the presence of domain boundaries formed by merged Cu(110)–(2 × 1)–O mismatched rows results in preferred oxygen adsorption at the tetrahedral sites in between the topmost and second outermost atomic layers at the oxygen coverage θ = 0.53 and the second and third outermost atomic layers at θ = 0.56. The bond length and angle of the resulting Cu–O tetrahedra resemble that of the Cu_2O structure, an indication of the onset of internal oxidation. Our results demonstrate that the presence of defects in an oxygen chemisorbed layer enables subsurface oxygen adsorption induced bulk-like oxide formation, thereby bypassing the higher-oxygen coverage surface restructuring of the Cu(110)–$c(6 \times 2)$ by on-surface oxygen adsorption for a non-defective (2 × 1)–O area.

II. COMPUTATIONAL METHOD

The DFT calculations are performed using the Vienna *ab-initio* simulation package (VASP)[59–62] with the PW91 generalized gradient approximation (GGA)[63] and projector augmented wave (PAW)[64,65] potentials. A cutoff energy of 380 eV is used and confirmed to give a converged adsorption energy from previous work.[66] We also performed a separate cutoff energy test, using cutoff energies of 380 eV and 450 eV, by adsorbing an oxygen atom on the surface in the middle of our super cell, and found that the difference in adsorption energy was only 0.02 eV, so we conclude an energy cutoff of 380 eV is sufficient. The Brillouin-zone integration is performed using (3 × 2 × 1) K-point meshes based on Monkhorst-Pack grids[67] and with broadening of the Fermi surface according to Methfessel-Paxton smearing technique[68] with a smearing parameter of 0.2 eV. We calculated the lattice constant of Cu to be 3.64 Å, which is in good agreement with previous calculations.[21,54,69] The surface is modeled by a periodically repeated slab consisting of five layers with the bottom two layers fixed, while the other layers are free to relax until all force components acting on the atoms are below 0.015 eV/Å, and successive slabs are separated by a vacuum region of 12 Å.

We applied the climbing image nudged elastic bands (CI-NEB) method[70] to calculate the reaction barriers, where

we used five intermediate images between the initial and final states. We investigate the oxygen adsorption energies and surface morphology changes in sequence using a single adsorbed oxygen atom for each calculation. The most stable configuration identified after an oxygen atom has been adsorbed is used as the reference for the next oxygen atom to be adsorbed. The oxygen adsorption energy E_{ads} is calculated using the equation

$$E_{ads} = \frac{1}{N_O}(E^{tot}_{O/Cu} - E_{ref} - \frac{N_O}{2}E_{O_2}), \quad (1)$$

where $E^{tot}_{O/Cu}$ is the total energy of the Cu–O system, and E_{ref} is the energy of the structure that we use as a reference to compare the relative stability, and more specifically, it is the total energy of the most stable configuration with one fewer subsurface oxygen atom compared with the system under study. E_{O_2} is the energy of an isolated oxygen molecule and N_O is the number of oxygen atoms newly adsorbed into the system, which is equal to 1 throughout this work for sequentially increasing the oxygen coverage by a single oxygen atom. We have also calculated the formation energy ΔE of the domain boundary by the following equation:

$$\Delta E = \frac{(E_{Shift} - E_{2\times1} - N_{atom}E_{atom})}{SA}, \quad (2)$$

where E_{Shift} is the total energy of the slab with the domain boundaries, $E_{2\times1}$ is the total energy of the slab with the perfect (2×1)–O surface, E_{atom} is the energy of either a Cu atom in the bulk, calculated by dividing the total energy of Cu atoms in a bulk system by the number of Cu atoms in the cell, or a single O atom from an isolated O_2 molecule, N_{atom} is the number of Cu or O atoms added to the system in the slab with the domain boundaries, and SA is the surface area. For the O-only boundary, there are four more O atoms than the perfect (2×1)–O surface, and for the Cu-only boundary, there are four more Cu atoms. The atomic structures are visualized using the XCrySDen package.[71]

III. RESULTS AND DISCUSSION

Upon oxygen exposure, Cu(110) develops into a well ordered (2×1)–O reconstruction with an oxygen coverage $\theta = 1/2$. In this oxygen-chemisorbed added-row reconstruction, Cu–O–Cu chains are aligned along the [001] direction of the Cu(110) substrate in every other [110]–(1×1) spacing, where the O atoms are positioned at the long bridge sites between Cu atoms.[41,43] Shown in Fig. 1(a) is a surface structural model of the Cu(110)–(2×1)–O perfect added row structure with the saturated oxygen coverage of $\theta = 1/2$. For all of our figures, the bigger blue balls represent Cu atoms, while the smaller red balls represent O atoms. The coverage is defined as the ratio of the number of oxygen atoms over the number of the Cu atoms in the corresponding clean surface. For the Cu(110)–(2×1)–O reconstructed surface, there is a Cu–O–Cu row along the [100] direction in every other spacing. Every other row that does not contain the Cu–O–Cu chains is vacant. The random process of nucleating Cu–O–Cu chains across the surface terrace can result in misaligned (2×1)–O domains, i.e., the Cu–O–Cu chain of the domain is aligned with the vacant row of the adjacent domain. Therefore, a domain boundary develops by shifting the Cu–O–Cu rows by half the distance (i.e., one [110] lattice spacing) between the Cu–O–Cu rows in the direction that is perpendicular to the Cu–O–Cu chains, so that the chains are still parallel to each other. Note that it is not possible for the Cu–O–Cu chains to be perpendicular to each other because the Cu(110) surface is not isotropic. While six different domain boundaries can develop for the missing rows of the oxygen-chemisorbed $(2\sqrt{2}\times2\sqrt{2})$ R45°–O reconstruction in Cu(100)[31] due to the difference in missing rows and the 4-fold symmetry of the (100) surface, only 2 domain boundary structures, i.e., boundary consisting of all Cu atoms and boundary consisting of all O atoms, can develop for the (2×1)–O reconstruction of Cu(110) owing to its lower symmetry (i.e., 2-fold symmetry). We calculated the formation energies of the Cu-only and O-only boundaries, which are 0.0115 eV/Å^2 and −0.005 eV/Å^2, respectively. The formation energy for the Cu-only boundary is slightly positive, suggesting that its formation is thermodynamically unfavorable compared to the perfect (2×1)–O structure and the O-only boundary. However, Cu-only boundaries can still exist because they are formed from the merging of randomly nucleated and shifted Cu–O–Cu chain fragments, which also suggests that the presence of the different boundary structures is random. Although the two types of the domain boundaries

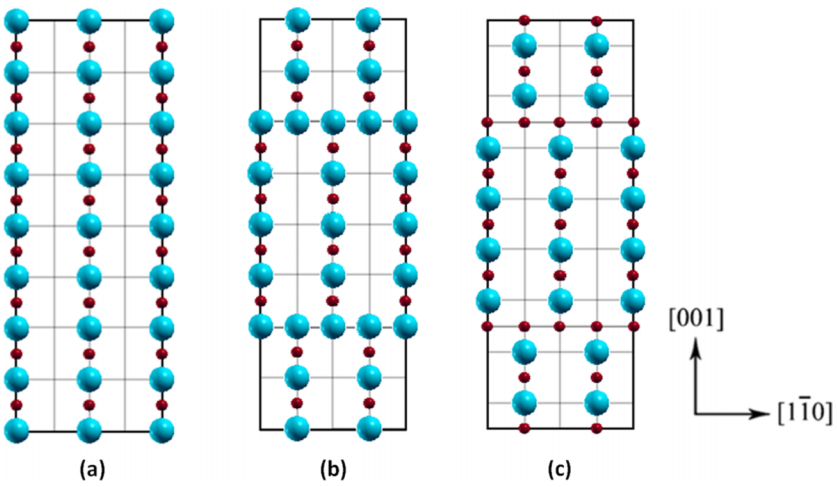

FIG. 1. Structural models of the Cu(110)–(2 × 1)—O reconstructed surfaces and the supercells used in our DFT calculations. (a) Perfect added row, (b) boundary consisting of all Cu atoms, and (c) boundary consisting of all O atoms.

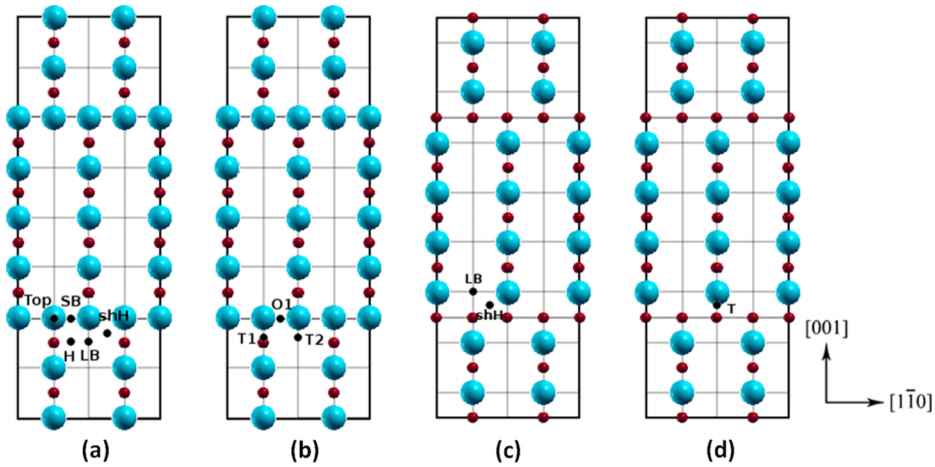

FIG. 2. Structural model of the Cu(110)—(2 × 1)—O surfaces with mismatched rows and the approximate locations of the possible ((a), and (b)) on-surface adsorption sites and subsurface adsorption sites for the boundary consisting of all Cu atoms; ((c), and (d)) on-surface adsorption sites and subsurface adsorption sites for the boundary consisting of all O atoms.

are not equally stable, transformation from one boundary to the other can be kinetically hindered because of the required massive structure change involved. Therefore, once a boundary is formed from merging Cu–O–Cu chain fragments, it will persist even it is thermodynamically unfavorable.

Our supercells are constructed with a domain boundary as shown in Figs. 1(b) and 1(c). The supercell is constructed with two boundaries. To eliminate any interaction between the two boundaries, we have to create a cell of sufficient size. We compare the on-surface oxygen adsorption energy on a hollow site halfway between the boundaries formed by Cu atoms of the boundary cell with a hollow site of the perfect added-row supercell. The energy difference is about 0.03 eV, indicating that the size of our constructed supercell is sufficient so that any boundary-boundary interaction has negligible effect for the cells. Our supercell with the boundary formed by Cu contains 148 Cu atoms and 16 O atoms, while the supercell with the boundary formed by O contains 144 Cu atoms and 20 O atoms.

We first examine both the on-surface and subsurface sites for the adsorption of oxygen atoms. We do this by calculating the oxygen atom adsorption energy for each on-surface and subsurface adsorption site in the domain boundary area. We consider the possible oxygen adsorption sites within one atomic displacement in the [001] direction, perpendicular to the domain boundary because the sites located more than one atomic displacement away from the boundary have the similar oxygen adsorption behavior as that of the perfect added-row structure and are thus not considered. Fig. 2(a) shows the possible sites for on-surface oxygen atom adsorption while Fig. 2(b) shows the sites for subsurface oxygen atom adsorption on the Cu(110)–(2 × 1)–O surface with mismatched Cu–O–Cu rows for the boundary consisting of Cu atoms only. On the surface of the reconstructed Cu(110), within one atomic displacement, there are five distinct on-surface oxygen adsorption sites. The hollow site (H) is located above the center of four surface Cu atoms, the long-bridge site (LB) is located between pairs of surface Cu atoms along the [110] direction. For binding sites that are along the Cu–O–Cu chains, but have one vacant Cu, we still use the term LB to describe those sites for simplicity. The short-bridge (SB) sites are located between pairs of surface Cu atoms along the [001] direction. The shifted-hollow (shH) site is a pseudo threefold coordinated and is located about half-way between the hollow and short-bridge sites. Finally, the top (Top) site is direct above a surface Cu atom and has been shown to be unstable,[64] and not further explored except for our first calculation as a test. The subsurface adsorption sites are the tetrahedral (T) site, which has a coordination number of 4, and the octahedral (O) site which has a coordination number of 6. We have only performed calculations regarding the subsurface sites that are located in the second outermost layer and have not considered the subsurface adsorption sites in third layer. All these sites for on-surface oxygen and subsurface adsorption are marked in Figs. 2(a) and 2(b). Note that no further oxygen adsorption calculations are performed for situations where the possible adsorption sites are near or at an existing oxygen atom since they are unstable sites for oxygen adsorption.

After relaxing the structures containing the Cu-only domain boundaries with a single oxygen atom at those potential adsorption sites, we find that there are two stable structures with similar oxygen adsorption energies for the Cu-only boundary cell, −1.98 eV and −2.13 eV. For both cases, the oxygen atom resides on the surface giving the surface oxygen coverage $\theta = 0.53$ for both structures, as shown in Table I. We will refer to each structure as Configuration A and Configuration B, shown in Figs. 3 and 4, respectively. For Configuration A, an oxygen atom initially at the LB site will stabilize at that site with an adsorption energy of −1.98 eV. As shown in Table I, on-surface oxygen atoms initially located at the H and shH sites will stabilize to the LB site, and an oxygen atom initially located at the T2 site will stabilize to the on-surface LB site, shown in Table I. The other two subsurface sites, O and T1, will stabilize in their initial subsurface positions, but have a higher adsorption energy (less negative) than that of the subsurface T2 site stabilizing to the on-surface LB site. For Configuration B, oxygen first adsorbs to the shifted-hollow site with an adsorption energy of −2.13 eV, which is lower than the adsorption energy of the first oxygen atom in Configuration A. There are no additional adsorption sites that eventually stabilize to the shH site, other than an oxygen atom at the shH site itself, which is unlike the case for the LB site.

Although the structure with an adsorbed oxygen atom at the shH is the most stable, the structure with an adsorbed oxygen atom at the LB site has a similar adsorption energy, so we cannot eliminate it as a possible final structure because of the closeness in oxygen adsorption energy, differing by

TABLE I. The adsorption energies of the first on-surface and subsurface oxygen atoms for both Cu-only and O-only domain boundaries. The oxygen coverage for the Cu-only and O-only boundaries are $\theta = 0.50$ and $\theta = 0.625$, respectively, before an oxygen atom is adsorbed. The abbreviations for the adsorption sites are defined in Fig. 2.

Cu-only boundary		
On-surface adsorption site	Adsorption energy (eV)	Stabilized site
SB	−0.18	
LB	−1.98	
Top	−1.98	LB
H	−1.98	LB
shH	−2.13	
Subsurface adsorption site	Adsorption energy (eV)	Stabilized site
O1	−1.00	
T1	−0.31	
T2	−1.97	LB
O-only boundary		
On-surface adsorption site	Adsorption energy (eV)	Stabilized site
H	−1.18	Away from boundary
shH	−1.18	Away from boundary
Subsurface adsorption site	Adsorption energy (eV)	Stabilized site
T	−1.18	To surface, away from boundary

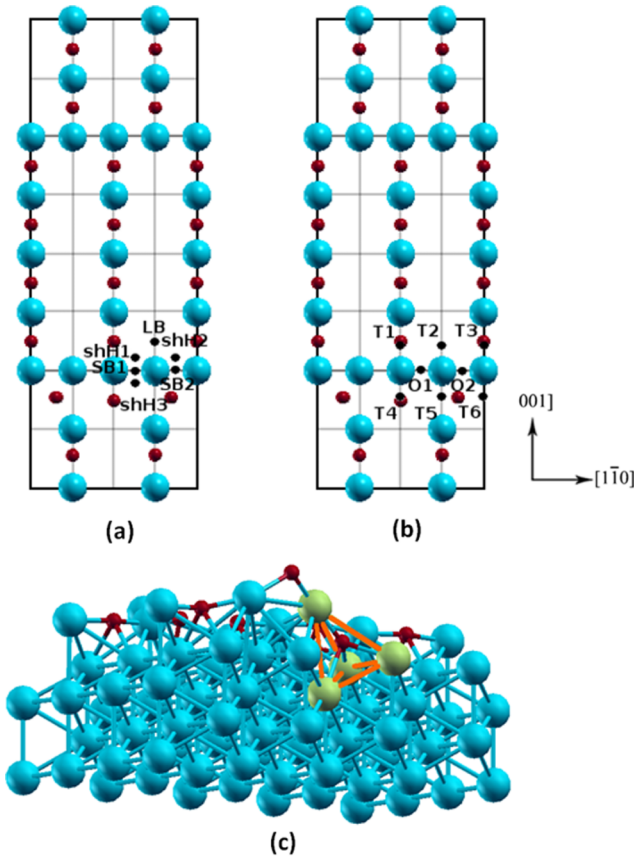

FIG. 3. Structural model of "Configuration A" and the approximate locations of the possible (a) on-surface adsorption sites and (b) subsurface adsorption sites. The equilibrium structure of the tetrahedron formed from the oxygen subsurface adsorption for the oxygen coverage $\theta = 0.53$. The resulting Cu_2O-like tetrahedron is highlighted in orange, in which the Cu atoms of the tetrahedron are represented by the green balls.

only 0.15 eV. Therefore, we consider both cases to continue for further oxygen atoms to be adsorbed to an on-surface or subsurface site.

The on-surface oxygen binding sites (SB, LB, Top, H, shH) apply for near the Cu-only boundary, but not at the O-only boundary. For this reason, we simply tested two arbitrary on-surface sites, a pseudo-hollow site and pseudo-long bridge site, shown in Fig. 2(c) acting as if the O-only boundary were made of Cu atoms instead. Fig. 2(d) shows the tetrahedral site, marked T. There are no octahedral sites located at the boundary, since the boundary consists of only O sites. We first relax the structure with the domain boundary consisting of only O atoms. For the two on-surface sites shown in Fig. 2(c), the oxygen adsorption energy is negative, as shown in Table I. However, the adsorbed oxygen in both cases diffuses further than one atomic displacement from the O-only boundary to the same location and stabilizes there. There is one subsurface adsorption site labeled T, in Fig. 2(d), that diffuses to the surface and stabilizes in the same location where the oxygen at H and shH stabilize. From these results, we can conclude that on-surface and subsurface oxygen adsorption is unstable near an O-only domain boundary of the Cu(110)–(2 × 1)–O surface.

A. Configuration A

We will continue with Configuration A to further adsorb oxygen atoms until the most stable adsorption site is found to be in the subsurface. Configuration A currently has an oxygen coverage of $\theta = 0.53$ (17 O atoms) and adsorbing an additional O atom to the surface would give an oxygen coverage of $\theta = 0.56$ (18 O atoms). Shown in Fig. 3 are both the on-surface and subsurface oxygen adsorption sites for Configuration A, which has an oxygen coverage of $\theta = 0.53$. There are more nonequivalent sites than previously shown in Fig. 2, due to the first oxygen atom adsorbing to the surface and causing a slight change to the structure. However, since the surface structure is still symmetrical, we only need to be concerned about half of the adsorption sites, as the other half will be equivalent sites. The adsorption energies for both on-surface and subsurface oxygen adsorption sites are shown in Table II. The most stable oxygen adsorption site resides in the subsurface, the tetrahedral site, with an adsorption energy of −1.88 eV. The oxygen atom initially placed at the O2 octahedral site stabilizes at the T2 tetrahedral site, indicating that there is a strong preference for oxygen adsorption at the tetrahedral site over the octahedral site in the presence of a domain boundary. We examine the atomic structure of the tetrahedra resulted from the most stable configuration in which the oxygen atom adsorbs to the T2 site, shown in Fig. 3(c). The bond lengths of the tetrahedron ranges from 1.82 Å to 2.044 Å and the Cu–O–Cu bond angles fall between 85.20° and 145.04°. Our DFT calculation found that the bond length and bond angle in

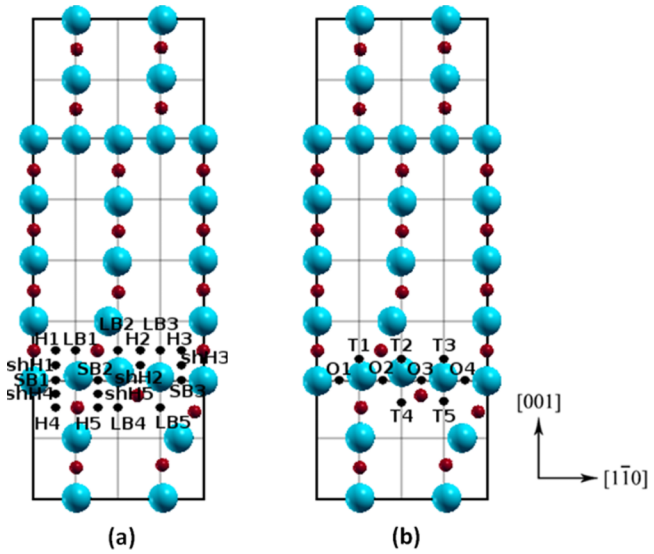

FIG. 4. Structural model of "Configuration B" and the approximate locations of the possible (a) on-surface adsorption sites and (b) subsurface adsorption sites.

bulk Cu_2O are 1.86 Å and 109.47°, respectively. Although the bond lengths of our tetrahedra are relatively close to the bond length in bulk Cu_2O, the bond angle discrepancy suggests that we have a distorted tetrahedral structure compared with the perfect Cu_2O tetrahedron that is found in the bulk oxide.

We employed the CI-NEB method to calculate the energy barrier for an oxygen atom to diffuse to the resulting subsurface tetrahedral site. We used the relaxed structure resulting from an oxygen adsorbed on the shH2 site as the initial state, while the final state is the oxygen adsorbed at the T2 site. The shH2 site is the most stable on surface site and happens to be located just above the T2 site. We determined the energy barrier to be 0.26 eV, lower than the barrier for the diffusion of atomic oxygen on Cu(110)–(2 × 1) chemisorbed layer along the [100] direction in between the Cu–O–Cu–O chains as the supply of extra oxygen to form the Cu(110)–c(6 × 2) phase, which is 0.53 eV.[69] The lower energy barrier indicates that it is more favorable for the on-surface oxygen atom to diffuse to the subsurface tetrahedral site than to diffuse along the Cu–O–Cu–O to form the Cu(110)–c(6 × 2) phase.

TABLE II. The adsorption energies of the on-surface and subsurface oxygen atoms. The oxygen coverage is θ = 0.53 before an oxygen atom is adsorbed. The abbreviations for the adsorption sites are defined in Fig. 3.

On-surface adsorption site	Adsorption energy (eV)	Stabilized site
SB1	−1.63	shH1
SB2	−1.47	shH2
LB1	−1.54	
LB2		
LB3		
shH1	−1.63	
shH2	−1.47	
shH3	0.11	
shH4	−1.21	
Subsurface adsorption site	**Adsorption energy (eV)**	**Stabilized site**
O1	−1.54	LB1
O2	−1.88	T2
T1	−0.40	
T2	−1.88	
T3	−0.36	
T4	−0.21	
T5	−0.42	
T6	−0.07	

B. Configuration B

We continue this investigation by adsorbing oxygen atoms onto the other stable structure found after the first oxygen is adsorbed. Shown in Fig. 4 are both the on-surface and subsurface oxygen adsorption sites for Configuration B, which has an oxygen coverage of θ = 0.53. Unlike Configuration A, Configuration B lacks symmetry, creating additional adsorption sites. The oxygen adsorption energies for both on-surface and subsurface oxygen adsorption sites are shown in Table III.

The most stable oxygen adsorption site is at the on-surface shH1 site with an adsorption energy of −1.83 eV. An oxygen initially placed at the H1 hollow site will stabilize to the

TABLE III. The adsorption energies of the on-surface and subsurface oxygen atoms. The oxygen coverage is θ = 0.53 before an oxygen atom is adsorbed. The abbreviations for the adsorption sites are defined in Fig. 4.

On-surface adsorption site	Adsorption energy (eV)	Stabilized site
SB1	−1.11	
SB2	−0.45	
SB3	−0.07	
LB1	−1.51	
LB2	−1.28	H2
LB3	−1.65	
LB4	0.38	
LB5	−1.33	Away from boundary
H1	−1.83	shH1
H2	−0.98	
H3	−1.65	LB3
H4	−0.23	
H5	0.01	
shH1	−1.83	
shH2	−1.65	LB3
shH3	−1.52	
shH4	−0.97	
shH5	−0.05	
Subsurface adsorption site	**Adsorption energy (eV)**	**Stabilized site**
O1	−0.65	
O2	−0.21	
O3	−0.33	
O4	−0.70	
T1	−0.55	
T2	−0.05	
T3	−1.39	
T4	0.02	
T5	−0.88	

TABLE IV. The adsorption energies of the on-surface and subsurface oxygen atoms. The oxygen coverage is θ = 0.56 before an oxygen atom is adsorbed. The abbreviations for the adsorption sites are defined in Figure 5.

On-surface adsorption site	Adsorption energy (eV)	Stabilized site
SB1	−0.17	O2
SB2	−0.34	O4
LB1	0.17	
LB2	−1.11	Away from boundary
LB3	−0.98	Away from boundary
H1	−0.02	
H2	−0.02	
shH1	−0.02	H1
shH2	−0.13	
shH3	−0.02	H2
shH4	−0.14	

Subsurface adsorption site	Adsorption energy (eV)	Stabilized site
O1	−0.66	
O2	−0.17	
O3	−0.66	
O4	−0.34	
T1	−0.34	O4
T2	0.06	
T3	−0.66	
T4	−0.66	
T5	0.30	
T6	−0.66	
T7	0.06	
T8	−0.34	O4

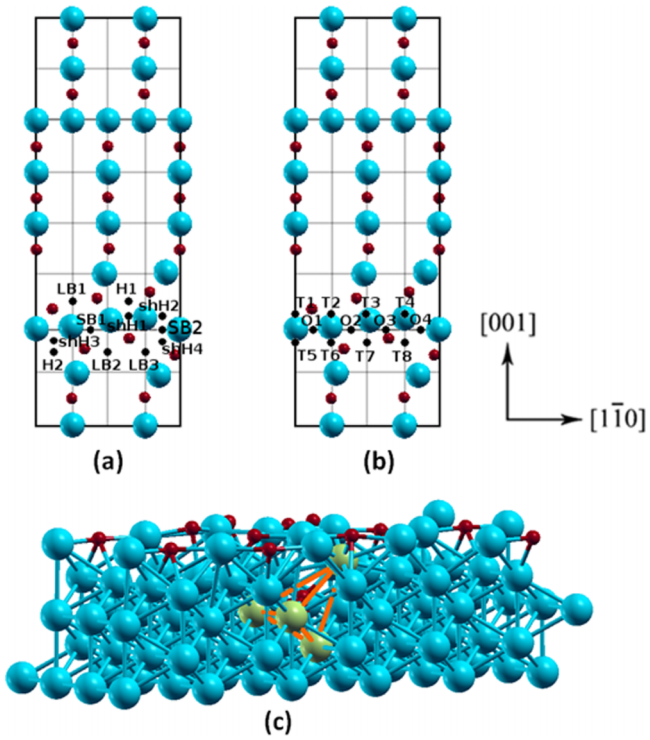

FIG. 5. Structural model of "Configuration B" with an additional adsorbed oxygen atom and the approximate locations of the possible (a) on-surface adsorption sites and (b) subsurface adsorption sites. (c) The equilibrium structure of the tetrahedron formed from the oxygen subsurface adsorption for the oxygen coverage θ = 0.56. The resulting Cu_2O-like tetrahedron is highlighted in orange, in which the Cu atoms of the tetrahedron are represented by the green balls.

shifted-hollow site shH1. An oxygen initially placed at the LB5 long bridge site will move further from the boundary to more than 1 atomic displacement away from the boundary. The most stable subsurface adsorption site is at the T3 tetrahedral site with an adsorption energy of −1.39 eV. Overall, the configuration with the oxygen atom adsorbed at the shift-hollow site is more stable than that with the oxygen adsorbed at the tetrahedral site, so we use that structure to continue with the oxygen atom adsorption.

Figs. 5(a) and 5(b) show the on-surface oxygen adsorption sites and the subsurface adsorption sites for the next oxygen atom to be adsorbed, where the initial oxygen coverage on the surface for this structure is now θ = 0.56. Table IV shows the oxygen-adsorption energies for each of those sites. In the two most stable configurations, LB2 and LB3, with oxygen adsorption energies of −1.11 eV and −0.98 eV, respectively, the additional on-surface adsorbed oxygen appears to have diffused away from the domain boundary to further than one atomic displacement. Since this study concerns oxygen adsorption within one atomic displacement from the domain boundary, we choose to ignore these two on-surface adsorption sites. The next most stable adsorption site is a subsurface tetrahedral site, with an adsorption energy of −0.66 eV for the O1, O3, T3, T4, and T6 sites.

Once again, it is found that a distorted tetrahedron is formed when the first oxygen atom is adsorbed into the subsurface. Oxygen adsorption at O1 and T6 sites results in the same final configuration, while oxygen adsorption at O3, T3, and T4 sites results in the same final configuration. All of the T adsorption sites in our calculations are initially in the second layer. Although the final position of the adsorbed oxygen is in a tetrahedron, the final position of the oxygen atom is not at one of the tetrahedral sites that we initially selected to be an oxygen adsorption site. Instead, the oxygen diffuses deeper into the bulk and embeds itself between the second and third outermost layers, where the Cu–O tetrahedron is formed, rather than in the second layer, as we selected for our initial oxygen adsorption site. These results show that the tetrahedral site is energetically favorable compared to the octahedral site in the presence of a domain boundary.

We performed three different CI-NEB calculations to determine the energy barrier for an oxygen atom to diffuse to the resulting subsurface tetrahedral site using three different initial states. We used the relaxed structures resulting from an oxygen adsorbed on the H1, shH2, and shH4 for the initial states, while the final state for each calculation is the relaxed structure with an oxygen adsorbed at T3. The shH2 and shH4 sites are the most stable on surface sites, but have long diffusion paths, so we also included the structure with the oxygen adsorbed at the H1 site, which is above the T3 site. We determined the energy barriers for an oxygen atom to diffuse from the H1, shH2, and shH4 sites to be 0.93, 0.52, and 0.51 eV, respectively. The energy barrier for diffusion of atomic oxygen from shH2 and shH4 sites are comparable to the barrier for the diffusion of atomic oxygen on Cu(110)–(2 × 1)

chemisorbed layer along the [100] direction in between the Cu–O–Cu–O chains as the supply of extra oxygen to form the Cu(110)–$c(6 \times 2)$ phase, which is 0.53 eV.[69] Although the energy barrier for an oxygen atom at the H1 site to diffuse to the T3 site is higher than the barrier for atomic oxygen diffusion along the chains, it is still lower than the barrier of 1.41 eV for the concerted movement of Cu atoms involved in the Cu(110)–(2×1) to Cu(110)–$c(6 \times 2)$ transition,[69] so it is more likely for the oxygen atom to diffuse to the subsurface tetrahedral site, than for the concerted movement of Cu atoms to take place.

We examine the atomic structure of the tetrahedron resulting from the most stable configurations. The bond lengths of the tetrahedron resulting from the stabilized structure in Configuration B range from 1.96 Å to 2.06 Å and the Cu–O–Cu bond angles fall between 85.93° and 123.23°, compared to bond lengths ranging from 1.82 Å to 2.04 Å and bond angles ranging from 82.2° to 145.04° of the tetrahedron resulted from the stabilized structure in Configuration A. The oxygen atom in the tetrahedron of Configuration B is located between the second and third layer, deeper than that of Configuration A, which is located in the second layer. To ensure that the presence of the bottom layer did not have significant contribution to the adsorption energy or configuration on the adsorbed subsurface oxygen atom, we performed a test using seven layers with the bottom two layers fixed. The difference in adsorption energy, using five layers versus seven layers, of the deepest adsorbed subsurface oxygen atom (between second and third layer) is only 0.01 eV, and the difference in bond angles remain unchanged, while the bond lengths changed by less than 1%. From this test, we conclude that our five layer slab is thick enough to neglect the presence of the bottom layer.

By comparing the bond length and bond angles of the two tetrahedra formed in both Configuration A and Configuration B, we can see that the bond lengths are similar, but the bond angles are significantly different. The bond angles in the tetrahedron in Configuration B more closely resembles the tetrahedron structure found in the bulk oxide, and the tetrahedron is formed deeper into the bulk in Configuration B than in Configuration A. These differences may be attributed to the fact that the stabilized structure of Configuration B, after a subsurface tetrahedron has been formed, has a higher oxygen coverage. The increased O–O repulsion at the surface at higher oxygen coverage may induce oxygen subsurface adsorption.[18,19,72,73] For a non-defective added-row region, further oxygen coverage for the Cu(110)–(2×1) phase leads to the transition to the Cu(110)–$c(6 \times 2)$ reconstructed surface via on-surface oxygen adsorption until reaching the oxygen coverage $\theta = 2/3$,[69] beyond which subsurface oxygen adsorption becomes energetically more favorable first at the octahedral sites and then at the tetrahedral sites when the oxygen coverage reaches $\theta = 1$.[58] In the presence of the domain boundary, we find that further oxygen coverage over $\theta = 0.53$ for the Cu(110)–(2×1) reconstruction in the domain boundary region results in subsurface oxygen adsorption and tetrahedral preference, for which the transition to the Cu(110)–$c(6 \times 2)$ reconstruction that requires further on-surface oxygen adsorption is bypassed. These results indicate that the presence of the domain boundary in the Cu(110)–(2×1) chemisorbed layer induces the formation of Cu_2O-like tetrahedra in the second and third atomic layer, which suggests that the onset of the internal oxidation can occur at very low oxygen coverage initiated at the defected region of the oxygen chemisorbed layer.

IV. CONCLUSION

By employing DFT calculations, we have examined the energetics of oxygen subsurface adsorption during the oxidation of Cu(110). Our results show that the oxidation of Cu(110) terrace is via a heterogeneous nucleation process, where the Cu-only boundaries formed by merged parallel missing-row domains with half unit-cell mismatch are preferred sites for forming Cu_2O-type Cu–O tetrahedra. The crossover from oxygen octahedral adsorption to tetrahedral adsorption may signal the onset of bulk oxide formation. The bond length and bond angles of the resulting distorted tetrahedra formed are calculated and are consistent with previous work performed on the domain boundaries in the missing-row reconstructed oxygen chemisorbed layer of Cu(100). The results obtained from this work are further evidence that the domain boundary defects formed in an oxygen chemisorbed layer may facilitate bulk oxide formation in the subsurface region.

ACKNOWLEDGMENTS

Research supported by the U.S. Department of Energy, Office of Basic Energy Sciences, Division of Materials Sciences and Engineering under Award No. DE-FG02-09ER46600. This work used the computational resources from the Extreme Science and Engineering Discovery Environment (XSEDE), which is supported by National Science Foundation Grant No. OCI-1053575.

[1]T. Huang and D. Tsai, Catal. Lett. **87**, 173 (2003).
[2]F. Jing, Y. Zhang, S. Luo, W. Chu, H. Zhang, and X. Shi, J. Chem. Sci. **122**, 621 (2010).
[3]N. Turro, S. O'Brien, B. White, M. Yin, A. Hall, D. Le, S. Stolbov, and T. Rahman, Nano Lett. **6**, 2095 (2006).
[4]H. Over, Y. D. Kim, A. P. Seitsonen, S. Wendt, E. Lundgren, M. Schmid, P. Varga, A. Morgante, and G. Ertl, Science **287**, 1474 (2000).
[5]K. Reuter, M. Scheffler, C. Stampfl, and M. V. Ganduglia-Pirovano, Surf. Sci. **500**, 368 (2002).
[6]S. Mrowec, Corros. Sci. **7**, 563 (1967).
[7]R. A. Rapp, Metall. Trans. A **15**, 765 (1984).
[8]A. Guerrero-Ruiz, L. Rodriguez-Ramos, and J. L. G. Fierro, Appl. Catal. **72**, 119 (1991).
[9]C. Fukuhara, H. Ohkura, Y. Kamata, Y. Murakami, and A. Igarashi, Appl. Catal., A **273**, 125 (2004).
[10]A. Atkinson, S. Barnett, R. J. Gorte, J. T. S. Irvine, A. J. McEvoy, M. Mogensen, S. C. Singhal, and J. Vohs, Nat. Mater. **3**, 17 (2004).
[11]C. I. Carlisle, T. Fujimoto, W. S. Sim, and D. A. King, Surf. Sci. **470**, 15 (2000).
[12]J. T. Stuckless, N. Al-Sarraf, C. E. Wartnaby, and D. King, J. Chem. Phys. **99**, 2202 (1993).
[13]W. A. Brown, R. Kose, and D. A. King, Chem. Rev. **98**, 797 (1998).
[14]N. Al-Sarraf, J. T. Stuckless, C. E. Wartnaby, and D. A. King, Surf. Sci. **283**, 427 (1993).
[15]J. T. Stuckless, C. E. Wartnaby, N. Al-Sarraf, S. J. Dixon-Warren, M. Kovar, and D. A. King, J. Chem. Phys. **106**, 2012 (1997).
[16]M. Todorova, W. X. Li, M. V. Gandglia-Pirovano, C. Stempfl, K. Reuter, and M. Scheffler, Phys. Rev. Lett. **89**, 96103 (2002).
[17]M. Todorova, K. Reuter, and M. Scheffler, Phys. Rev. B **71**, 195403 (2005).

[18]X. Duan, O. Warschkow, A. Soon, B. Delley, and C. Stampfl, Phys. Rev. B **81**, 75430 (2010).
[19]M. Y. Lee and A. J. H. McGaughey, Surf. Sci. **603**, 3404 (2009).
[20]M. Y. Lee and A. J. H. McGaughey, Surf. Sci. **604**, 1425 (2010).
[21]T. Kangas, K. Lassonen, A. Puisto, H. Pitkanen, and M. Alatalo, Surf. Sci. **584**, 62 (2005).
[22]T. Kangas and K. Lassonen, Surf. Sci. **602**, 3239 (2008).
[23]T. Fujita, Y. Okawa, Y. Matsumoto, and K. I. Tanaka, Phys. Rev. B **54**, 2167 (1996).
[24]F. Jensen, F. Besenbacher, E. Laegsgaard, and I. Stensgaard, Phys. Rev. B **41**, 10233 (1990).
[25]F. Besenbacher, Rep. Prog. Phys. **59**, 1737 (1996).
[26]J. K. Nørskov and F. Besenbacher, Prog. Surf. Sci. **44**, 5 (1993).
[27]M. Lampimaki, K. Lahtonen, M. Hirsimaki, and M. Valden, J. Chem. Phys. **126**, 034703 (2007).
[28]K. Lahtonen, M. Hirsimaki, M. Lampimaki, and M. Valden, J. Chem. Phys. **29**, 124703 (2008).
[29]W. W. Crew and R. J. Madix, Surf. Sci. **349**, 275 (1996).
[30]L. Guillemot and K. Bobrov, Phys. Rev. B **83**, 075409 (2011).
[31]L. Li, X. Mi, and G. W. Zhou, Phys. Rev. Lett. **108**, 176101 (2012).
[32]K. Reuter and M. Scheffler, Appl. Phys. A **78**, 793 (2004).
[33]E. Lundgren, G. Kresse, C. Klein, M. Borg, J. N. Andersen, M. De Santis, Y. Gauthier, C. Konvicka, M. Schmid, and P. Varga, Phys. Rev. Lett. **88**, 246103 (2002).
[34]M. Todorova, E. Lundgren, V. Blum, A. Mikkelsen, S. Gray, J. Gustafson, M. Borg, J. Rogal, K. Reuter, J. N. Andersen, and M. Scheffler, Surf. Sci. **541**, 101 (2003).
[35]E. Lundgren, A. Mikkelsen, J. N. Andersen, G. Kresse, M. Schmid, and P. Varga, J. Phys.: Condens. Matter **18**, R481 (2006).
[36]F. Jensen, F. Besenbacher, E. Laegsgaard, and I. Stensgaard, Surf. Sci. **259**, L774 (1991).
[37]F. Jensen, F. Besenbacher, and I. Stensgaard, Surf. Sci. **270**, 400 (1992).
[38]T. Matsumoto, R. A. Bennett, P. Stone, T. Yamada, K. Domen, and M. Bowker, Surf. Sci. **471**, 225 (2001).
[39]F. Yang, Y. M. Choi, P. Lui, D. Stacchiola, J. Hrbek, and J. A. Rodriquez, J. Am. Chem. Soc. **133**, 11474 (2011).
[40]J. K. Nørskov and K. W. Jacobsen, Phys. Rev. Lett. **65**, 1788 (1990).
[41]F. Jensen, F. Besenbacher, E. Laegsgaard, and I. Stensgaard, Phys. Rev. B **42**, 9206 (1990).
[42]R. Feidenhans'l, F. Grey, M. Nielsen, F. Besenbacher, F. Jensen, E. Laegsgaard, I. Stensgaard, K. W. Jacobsen, J. K. Nørskov, and R. L. Johnson, Phys. Rev. Lett. **65**, 2027 (1990).
[43]D. J. Coulman, J. Wintterlin, R. J. Behm, and G. Ertl, Phys. Rev. Lett. **64**, 1761 (1990).
[44]Q. Q. Liu, L. Li, N. Cai, W. A. Saidi, and G. W. Zhou, Surf. Sci. **627**, 75 (2014).
[45]J. I. Flege, J. Hrbek, and P. Sutter, Phys. Rev. B **78**, 165407 (2008).
[46]H. H. Kan and J. F. Weaver, Surf. Sci. **603**, 2671 (2009).
[47]R. B. Shumbera, H. H. Kan, and J. F. Weaver, Surf. Sci. **601**, 4809 (2007).
[48]J. F. Weaver, H. H. Kan, and R. B. Shumbera, J. Phys.: Condens. Matter **20**, 184015 (2008).
[49]G. W. Zhou and J. C. Yang, Phys. Rev. Lett. **89**, 106101 (2002).
[50]G. W. Zhou and J. C. Yang, Appl. Surf. Sci. **210**, 165 (2003).
[51]G. W. Zhou and J. C. Yang, Appl. Surf. Sci. **222**, 357 (2004).
[52]G. W. Zhou and J. C. Yang, Surf. Sci. **531**, 359 (2003).
[53]G. W. Zhou, L. Wang, and J. C. Yang, J. Appl. Phys. **97**, 063509 (2005).
[54]S. Y. Liem, G. Kresse, and J. H. R. Clarke, Surf. Sci. **415**, 194 (1998).
[55]S. Y. Liem, J. H. R. Clarke, and G. Kresse, Surf. Sci. **459**, 104 (2000).
[56]F. Frechard and R. A. van Santen, Surf. Sci. **407**, 200 (1998).
[57]B. G. Briner, M. Doering, H. -P. Rust, and A. M. Bradshaw, Phys. Rev. Lett. **78**, 1516 (1997).
[58]L. Li and G. W. Zhou, Surf. Sci. **615**, 57 (2013).
[59]G. Kresse and J. Hafner, Phys. Rev. B **47**, 558 (1993).
[60]G. Kresse and J. Hafner, Phys. Rev. B **49**, 14251 (1994).
[61]G. Kresse and J. Furthmüller, Comput. Mater. Sci. **6**, 15 (1996).
[62]G. Kresse and J. Furthmüller, Phys. Rev. B **54**, 11169 (1996).
[63]J. P. Perdew, K. A. Jackson, M. R. Pederson, D. J. Singh, and C. Fiolhais, Phys. Rev. B **46**, 6671 (1992).
[64]G. Kresse and D. Joubert, Phys. Rev. B **59**, 1758 (1999).
[65]P. E. Blöchl, Phys. Rev. B **50**, 17953 (1994).
[66]G. W. Zhou, L. Luo, L. Li, J. Ciston, E. Stach, and J. C. Yang, Phys. Rev. Lett. **109**, 235502 (2012).
[67]H. J. Monkhorst and J. D. Pack, Phys. Rev. B **13**, 5188 (1976).
[68]M. Methfessel and A. Paxton, Phys. Rev. B **40**, 3616 (1989).
[69]L. Li, Q. Q. Liu, J. Li, W. A. Saidi, and G. W. Zhou, J. Phys. Chem. C **118**, 20858 (2014).
[70]G. Henkelman, B. P. Uberuaga, and H. Jonsson, J. Phys. Chem. C **113**, 9901 (2000).
[71]A. Kokalj, Comput. Mater. Sci. **28**, 155 (2003).
[72]A. Soon, M. Todorova, B. Delley, and C. Stampfl, Phys. Rev. B **73**, 165424 (2006).
[73]S. Jaatinen, J. Blomqvist, P. Salo, A. Puisto, M. Alatalo, M. Hirsimaki, M. Ahonen, and M. Valden, Phys. Rev. B **75**, 75402 (2007).